Stability of Buoyancy-Induced Flows Adjacent to a Vertical Isothermal Surface in Cold Pure Water

-Neutral Stability in the Range $0 \leq R \leq 0.1515$-

Young-Kyu Hwang*

(Received March 20, 1996)

Numerical solutions of the hydrodynamic stability equations for buoyancy-induced flows adjacent to a vertical, planar, isothermal surface in cold pure water have been obtained for various values of the density extremum parameter $R = (T_m - T_\infty)/(T_0 - T_\infty)$. The present numerical study yields neutral stability results for the region of the flows corresponding to $0.0 \leq R \leq 0.1515$, where outside buoyancy force reversals arise. Also, it includes the relative stability of the three previously predicted multiple, steady-state solutions of the flow. When the stability results of the present work are compared to the previous experimental data, the numerical results agree well qualitatively.

Key Words : Neutral Stability, Outside Buoyancy Force Reversal, Density Extremum Parameter

Nomenclature

B	: Frequency parameter
B^*	: B at G_{cr}
c	: Wave speed
D	: Characteristic length
$f(\eta)$	: Generalized stream function
f	: Physical frequency
g	: Acceleration due to gravity
G	: Modified Grashof number, $4(Gr_x/4)^{1/4}$
G_{cr}	: Critical Grashof number
$Gr(x)$	: Local Grashof number
$H(\eta)$	: Nondimensional disturbance pressure amplitude funtion
$\bar{H}(y)$	: Disturbance pressure amplitude function
i	: $\sqrt{(-1)}$
k_1, k_2	: Constants
M	: Largest magnitude of any of the eigenvector components
Pr	: Prandtl number
q	: Exponent in the density relation of Gebhart and Mollendorf(1977)
R	: Density extremum parameter
$S(\eta)$	: Nondimensional disturbance temperature amplitude function
$S(y)$	: Disturbance temperature amplitude function
T	: Temperature
U	: Characteristic velocity
$W'(\eta)$	: Nondimensional local buoyancy force
x, y	: Coordinates
Z_0	: Coefficient in the stability equation, $\delta q\lvert\theta_b - R\rvert^{q-1}(\theta_b - R)/\lvert\theta_b - R\rvert$

Greek symbols

α	: Complex wave number, $\alpha_R + i\alpha_I$, $\alpha = \alpha_R$ for neutral stability
α^*	: α at G_{cr}
α_T	: Thermal expansion coefficient in the density relation of Gebhart and Mollendorf (1977), $(^\circ C)^{-q}$
β	: Disturbance frequency
δ	: $+1.0$ for upflow, -1.0 for downflow
δ_T	: Thermal boundary layer (in Fig. 2)
$\eta(x, y)$	: Similarity variable
$\eta_{p.i}$	: Points of inflection in the velocity profile

* Department of Mechanical Design, Sung Kyun Kwan University, Suwon 440-746, Korea.

$\theta(\eta)$: Nondimensional temperature, $(T - T_\infty)/(T_0 - T_\infty)$
ν : Kinematic viscosity
ρ : Density
$\Phi(\eta)$: Nondimensional disturbance velocity amplitude function
$\bar{\Phi}(y)$: Disturbance velocity amplitude function
$\Psi(x, y)$: Stream function

Subscripts

b : Base flow property
m : At the extremum condition
I : Imaginary
0 : Surface condition
R : Real
∞ : At ambient condition

Other Symbols

$\tilde{\ }$: Dimensional quantity

1. Introduction

The existence of a density extremum near 4℃ dramatically affects the characteristics of buoyancy induced flows in the cold pure water (Gebhart, 1979; Gebhart, et al. 1988). The occurrence of bi-directional buoyancy forces in the thermal boundary layer complicates their stability analyses. This study is the continuation of Hwang et al. (1993) to analyze the neutral stability of laminar vertical natural convection flows in the cold pure water in the presence of buoyancy force reversals. In this part, we first treat the case of upflow, i. e., outside buoyancy force reversals.

Our results are very accurate because, in contrast to the previous works obtained by the method of simple shooting (e. g., Higgins and Gebhart, 1983; Qureshi and Gebhart, 1986), the stability equations has been solved using an adequate computing code (COLNEW) designed to accurately solve two-point boundary-value problems (Ascher et al., 1981; Bader and Ascher, 1985). Moreover, our results are new in that we have analyzed the neutral stability of three multiple steady-state solutions found in this problem by El Henawy et al. (1982).

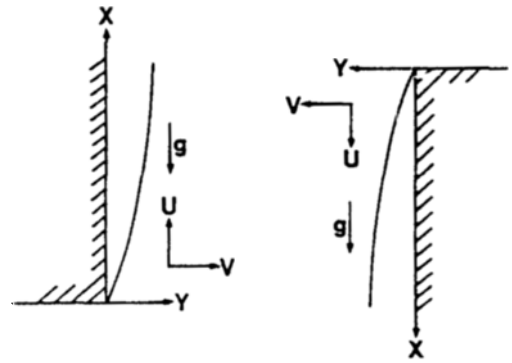

(a) Upflow (b) Downflow

Fig. 1 The coordinate systems

Most of the past stability studies has utilized the Boussinesq formulation of the density as a linear function of temperature, such as for flows in air, warm water etc. Recently, Gebhart and Mahajan (1982) and Gebhart et al. (1988) have comprehensively summarized the literature in this regard.

In the present study, the system under consideration (as seen in Fig. 1) is quiescent, cold, pure water adjacent to a vertical, planar, isothermal, impermeable surface. In this situation the Boussinesq approximation does not accurately express the buoyancy force.

This is due to the existence of the density extremum of cold water (its density is maximum at $T_m = 4.029325$℃ at 1 bar) in the thermal boundary layer. A considerable buoyancy force reversal arises across the thermal boundary layer. To predict the resulting subtle flow patterns, the following density extremum parameter was defined by Gebhart and Mollendorf(1978)

$$R = \frac{T_m - T_\infty}{T_0 - T_\infty} \tag{1}$$

where T_0 and T_∞ are the temperature of the isothermal surface and the temperature of the ambient medium (cold pure water), respectively.

The analysis of the steady-state flows in the presence of buoyancy force reversals in the range of $0 \leq R \leq 0.5$ is complex. To save space, we only refer to Wilson and Vyas (1979), Carey and

Gebhart (1981) for the experimentally observed flows, El-Henawy et al. (1982), Gebhart and Mollendorf (1978), and Carey et al. (1980) for the representation of similarity solutions for such flows.

This study is concerned principally with the presentation, for various values of the density extremum parameter R in the range of $0 \leq R \leq 0.1515$, of numerical results that predict realistic physical conditions of neutral stability for the base flow generated by natural convection adjacent to a vertical, isothermal plate (as seen in Fig. 1) in cold pure water.

The hydrodynamic stability of these base flows is of special interest, since under these conditions outside buoyancy force reversals (such as those seen in Fig. 2) exert strong influence upon the flow and the multiple-steady-state solutions of El-Henawy et al. (1982) are predicted to exist. Up to the three steady-states exist at the same R for the flow (as seen in Fig. 3), in the range $0.15149 \leq R \leq 0.15180$. Their influence on instability will be shown later.

The numerical study of the hydrodynamic stability for non-Boussinesq situations is difficult as mentioned by Hwang et al. (1993). The difficulty exists partly because the base flow itself is sensitive to buoyancy force reversal via the nonlinear buoyancy-force term in the mathematical model. An additional significant difficulty may come from the presence of a singularity in the linear stability equations as used by Qureshi (1980) and Higgins (1981); see also, Higgins and Gebhart (1983) and Qureshi and Gebhart (1986). Thus, reformulated stability equations of Hwang et al. (1993) to be solved is required in order to make them nonsingular.

Due to the difficulties mentioned above, most of the previous numerical studies were limited to the stability analyses for the simple cases of unidirectional buoyancy-induced flow : Higgins(1981) for several values of R with $1.0 \leq R \leq 8.0$, $R=0.4$, and $R=-0.5$ (see also Higgins and Gebhart, 1983); Qureshi (1980) for $R=0$ (see also Qureshi and Gebhart, 1986).

Hwang et al. (1993) obtained rather complete neutral stability results for the downflow in the

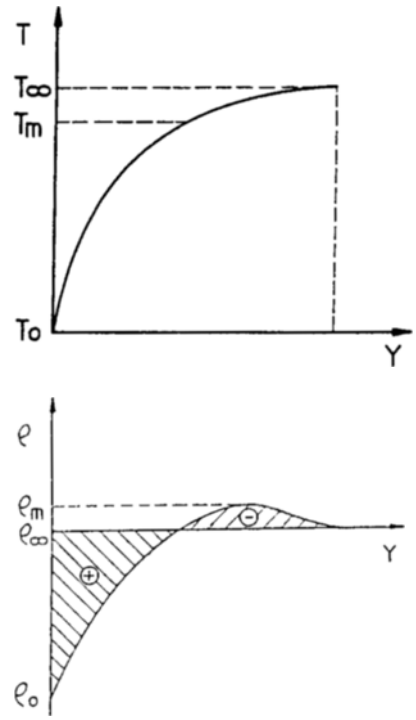

Fig. 2 Illustration of density behavior near T_m ; R 0.1, outside buoyancy force reversal.

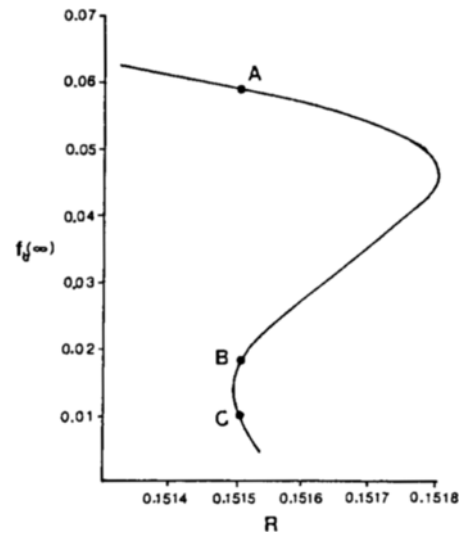

Fig. 3 Detail of the variation of mass-flow rate $f_b(\infty)$ with R. The marks A, B, and C correspond to the three multiple-steady-state solutions for the base flow at $R=0.1515$. From El-Henawy et al.(1982)

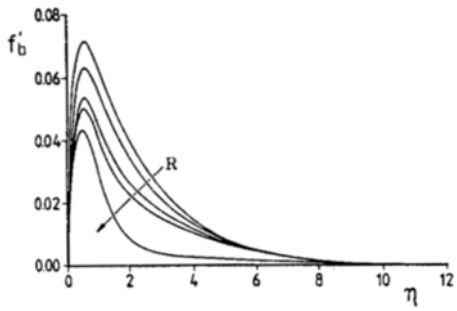

Fig. 4 Distributions of vertical velocity components $f_b'(\eta)$ of the base flows. The arrow indicates increasing $R=0.0$, 0.05, 0.10, 0.11667 and 0.15

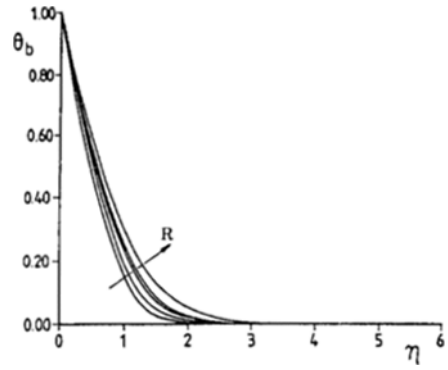

Fig. 5 Distribution of normalized temperature $\theta_b(\eta)$ of the base flow. The arrow indicates increasing $R=0.0$, 0.05, 0.10, 0.11667 and 0.15

range of $0.29181 \leq R \leq 0.5$, where inside buoyancy force reversals arise. They found that an increase in the magnitude of inside buoyancy force reversals, which were associated with the locations of the two points of inflection in the vertical velocity components of base flow, always caused the flows to be significantly more unstable.

The experimental studies by Higgins and Gebhart (1982) and Qureshi and Gebhart (1981) in cold water indicated that the density extremum behavior was found to delay transition, compared to the results in the water at room temperature.

The present numercal study includes neutral stability results for the region of the base flows corresponding to $0.0 \leq R \leq 0.1515$ for $Pr=11.6$. In particular, neutral stability curves are obtained at $R=0.1515$ for the three steady-states of the base flow which were found by El-Henawy et al. (1982). The effect of outside buoyancy force reversals on instability will be shown.

2. The Governing Equations

2.1 Base flow

The similarity equations for steady laminar base flows (with the coordinate definitions in Fig. 1) are well known; for example, El-Henawy et al. (1982), Gebhart and Mollendorf (1978), and Carey et al. (1980). To formulate them the following nondimensional quantities were used: η(a similarity variable), $f_b(\eta)$(stream functioin), and $\theta_b(\eta)$ (temperature), where

$$\eta=\frac{yG}{4x}, \quad \Psi_b(x,y)=\nu G f_b(\eta)$$
$$\theta_b(\eta)=\frac{T-T_\infty}{T_0-T_\infty} \tag{2a}$$

and

$$G=4\left(\frac{1}{4}Gr(x)\right)^{\frac{1}{4}}$$
$$Gr(x)=\frac{gx^3}{\nu^2}\alpha_T|T_0-T_\infty|^q \tag{2b}$$

Here α_T and q are the thermal expansion coefficient and exponent, respectively, from the density relation of Gebhart and Mollendorf (1977). For conditions at 1 bar pressure and no salinity in the range of temperature $0 \leq T \leq 20$℃, $\alpha_T=9.297173 \times 10^{-6}(℃)^{-q}$ and $q=1.894816$. The equations for the base flow in similarity form are:

$$f_b'''+3f_bf_b''-2f_b'^2 + \delta\{|\theta_b-R|^q-|R|^q\}=0 \tag{3a}$$
$$\theta_b''+3Prf_b\theta_b'=0 \tag{3b}$$

with boundary conditions

$$f_b'(0)=f_b(0)=f_b'(\infty) = \theta_b(0)-1=\theta_b(\infty)=0 \tag{4}$$

where $\delta=+1$ for upward flow, $\delta=-1$ for downward flow; see Gebhart and Mollendorf (1978). Pr=11.6 is the Prandtl number for cold pure water.

Here we only considered upward flows in the range $0.0 \leq R \leq 0.1515$, where outside buoyancy force reversals occured. The boundary-value problem (3a, b)~(4) was solved on intervals $[0, \eta_\infty]$ with $\eta_\infty = 23 \sim 300$ by using two computer codes: COLNEW (Ascher et al., 1981; Bader and Ascher, 1985) and BOUNDS (Deuflhard and Bader, 1982). Examples of dimensionless vertical velocity and temperature profiles for $0 \leq R \leq 0.15$ are given in Figs. 4 and 5, respectively. Also, Figure 6 from El-Henawy et al. (1982) shows the velocity profiles of the three multiple-steady-state solutions for the base flow at $R = 0.1515$.

Buoyancy force reversals cause significant effects on hydrodynamic transport. As R increases from 0 to 0.15, the downward buoyancy force, near the outer edge of the thermal boundary layer increases. For multiple steady-states of the base flow, the downward buoyancy force, which becomes stronger, causes an outside flow reversal as R increases from 0.15 to 0.1515 as shown in Fig. 6.

As R increases from 0 to 0.1333, the location of the single point of inflection in the profiles of the vertical component of velocity shifts closer to the isothermal surface ($\eta = 0$); see Fig. 4 and Table 1. However, for $0.1333 \leq R \leq 0.15$, the location of point of inflection remains $\eta_{p.i} = 0.97$ and does not change singnificantly. But the value of its stress $-f_b''(\eta_{p.i})$ increases significantly as R increases.

The shift of the location of point of inflectioin associated with its strength might increase the limit of stability of flow, just as in the forced flow problems, which will be discussed later.

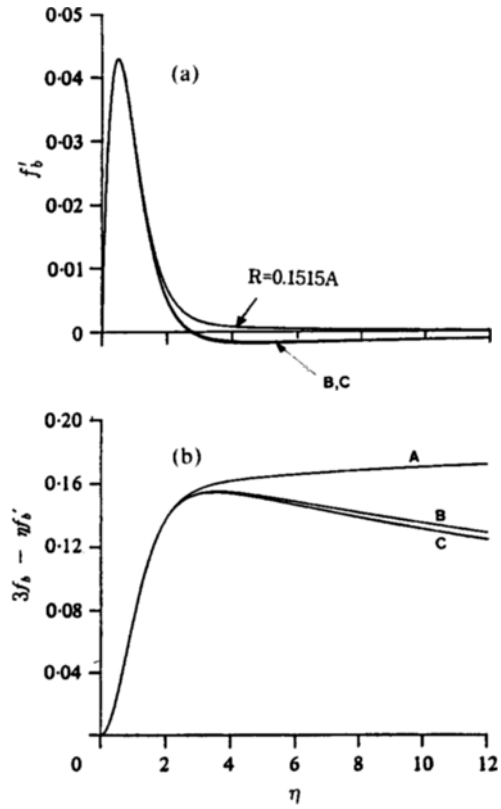

Fig. 6 The three multiple-steady-state solutions for the base flow at $R = 0.1515$, which correspond to 3 points in Fig. 3, in terms of (a) vertical velocity components f_b' and (b) horizontal velocity components $3f_b - \eta f_b'$. From El-Henawy et al.(1982)

2.2 The linear stability equation

A linear stability of two dimensional disturbances is considered. The disturbance quantities are normalized in the following manner, where D and U are the charactreristic length and velocity:

$$\Phi(\eta) = \frac{\bar{\Phi}(y)}{UD}, \quad S(\eta) = \frac{\bar{S}(y)}{T_0 - T_\infty}$$
$$H(\eta) = \frac{\bar{H}(y)}{\rho U^2}, \quad \alpha = \bar{\alpha} D, \quad \beta = \frac{\bar{\beta} D}{U}$$
$$D = \frac{4x}{G}, \quad U = \frac{\nu G^2}{4x} \tag{5}$$

The reformulated stability equations by Hwang et al. (1993) are used to avoid the singularity in buoyancy force term. The nonsingular Orr-Sommerfeld equations for buoyancy-induced flows are:

x-momentum,

$$(f_b' - c)\Phi' - f_b''\Phi = -H + \frac{1}{i\alpha G}(\Phi''' - \alpha^2\Phi' + Z_0 S) \tag{6a}$$

y-momentum,

$$(f_b' - c)\Phi = -\frac{H'}{\alpha^2} + \frac{1}{i\alpha G}(\Phi'' - \alpha^2\Phi) \tag{6b}$$

energy,

$$(f_b'-c)S-\theta_b'\Phi=\frac{1}{i\alpha G\mathrm{Pr}}(S''-\alpha^2 S) \quad (6c)$$

where $c=\beta/\alpha$, $\delta=+1.0$ for upflow and $\delta=-1.0$ for down flow, and

$$Z_0=\delta\frac{(\theta_b-R)}{|\theta_b-R|}q|\theta_b-R|^{q-1}$$

the nondimensional boundary conditions for an isothermal vertical surface are:

$$\Phi(0)=\Phi'(0)=S(0)=\Phi'(\infty)=S(\infty)=H(\infty)=0 \quad (7)$$

The linear stability Eqs. (6a~c) and (7) constitute a complex-valued, sixth-order, linear systems of homogeneous differential equations. The eigenvalues of the system are the nondimensional wave number α and frequency β. The ratio α/β is referred to as the wave speed c.

3. Numerical Method

To reduce the error propagation and to avoid the inaccuracy in simple shooting of Qureshi (1980) and Higgins (1981), the two-point-boundary-value-problem solver COLNEW (Ascher et al., 1981; Bader and Ascher, 1985) was used. With it we were able to compute the accurate numerical solutions of the stability equations in the range $0.0\leq R\leq 0.1515$. These could not be found by simple shooting.

To generate the families of solutions, two different ad hoc schemes were used. These are described below. Since there is no way to normalize the solutions of eigenvalue problem (6a~c) and (7) which is subject to homogeneous boundary conditions, an alternative must be found to avoid the trivial solution.

The first scheme, which succeeded, was to replace the boundary conditions $\Phi_R'(0)=\Phi_I'(0)=0$ by

$$S_R'(0)=k_1,\quad S_I'(0)=-k_2 \quad (8)$$

with $0.25\leq k_1\leq 1.0$ and $0.1\leq k_2\leq 1.0$. For moderate values of α and β, we use $k_1=k_2=1.0$. The computing procedure employed to use the orthogonal collocation code COLNEW for obtaining the neutral stability curve is described below. For a given value G, one guesses a pair of eigenvalues α and β. One then solves the boundary value problem (6a~c) and (7) with the modified boundary conditions (8), replacing $\Phi_R'(0)=\Phi_I'(0)=0$, using COLNEW, and iterates by adjusting the values of α and β until the boundary conditions $\Phi_R'(0)=\Phi_I'(0)=0$ are satisfied with $|\Phi_R'(0)|+|\Phi_I'(0)|\leq 10^{-6}$.

The second scheme is to add the trivial differential equations

$$\alpha'=0,\ \beta'=0 \quad (9)$$

to the system (6a~c) and to impose two nonzero conditions $S_R'(0)=-k_1$ and $S_I'(0)=-k_2$ in addition to (7). This scheme yields exact numerical solutions of the original eigenvalue problem (6a~c), (7) and (9). However, accurate initial guesses are required to get it to work.

When we used the first scheme, we insisted that, for a solution to be accepted, the following criteria were all met:

$$\min_{0\leq\eta\leq\eta_\infty}\left(\frac{|\Phi_R'(0)|}{|\Phi_R'(\eta)|},\ \frac{|\Phi_I'(0)|}{|\Phi_I'(\eta)|}\right)\leq 10^{-4} \quad (10a)$$

$$\max\left(\frac{|\Phi_R'(0)|}{M},\ \frac{|\Phi_I'(0)|}{M}\right)\leq 10^{-7} \quad (10b)$$

where M is the largest magnitude of any of the eigenvector components(i. e., Φ, Φ', Φ'', S, S', H) on $0\leq\eta\leq\eta_\infty$. In addition, the error estimates given on output by COLNEW are less than 10^{-4}.

The second scheme was used for the purpose of verification and improvement of the numerical results, which were obtained by the first scheme.

4. Numerical Results

Neutral stability results that have satisfied the standards for accuracy Eqs. (10. a~b) have been obtained for several values of R in the $0\leq R\leq 0.1515$. In particular, for $R=0.1515$, we obtained neutral stability curves for the three steady-states of the flow. These results are presented in Table 1 and Figs. 7~10.

Some of our numerical results on stability are presented in (G, B)-plane,
where

$$B=\beta G^{\frac{1}{3}}=\frac{2\pi f}{\nu}\left(\frac{g}{\nu^2}\alpha_T|T_0-T_\infty|^q\right)^{-\frac{2}{3}} \quad (11)$$

This parameter B has no x dependence; it is

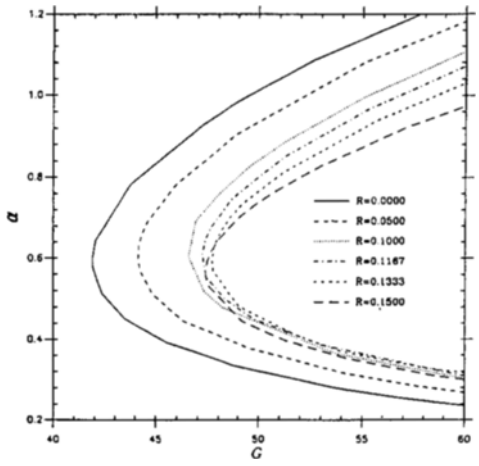

Fig. 7 Portions of computed neutral stability curves in the (G, α) plane

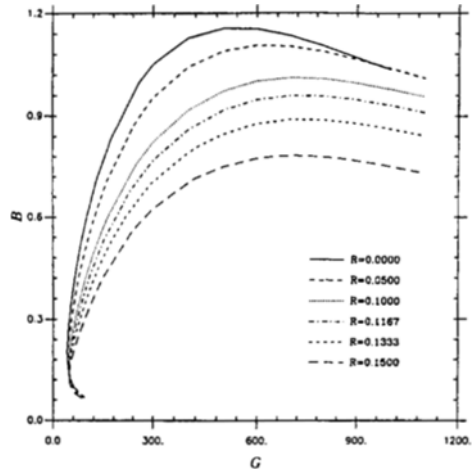

Fig. 9 Computed neutral stability curves in the (G, B) plane.

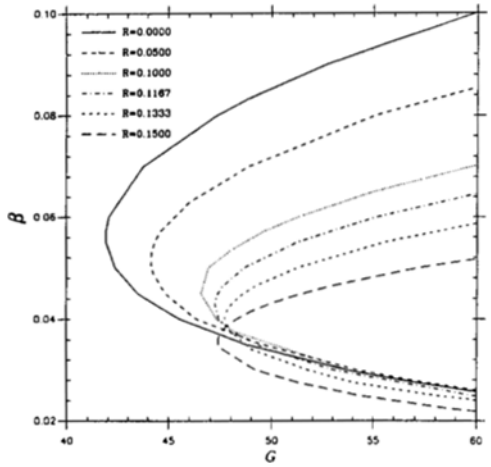

Fig. 8 Portions of computed neutral stability curves in the (G, β) plane.

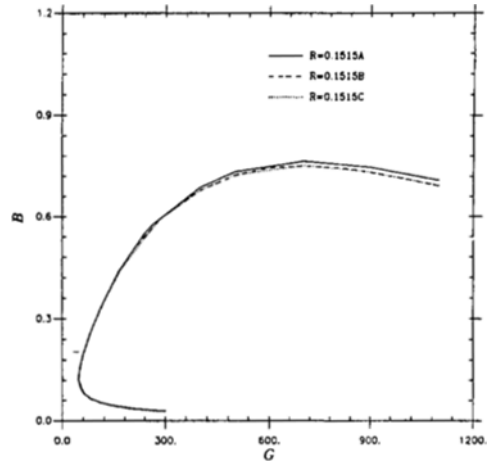

Fig. 10 Computed neutral stability curves in the (G, B) plane for the three steady-states of the base flow at $R=0.1515$

proportional to the physical frequency f. Constant frequency paths for G are horizontal straight lines in the (G, B)-plane; see Figs. 9 $\sim$10.

If $|T_0 - T_\infty|$ is fixed, a plot or a table in the neutral stability planes (i. e., (G, B) or (G, β)-plane also (G, α)-plane) is useful in quantitatively analyzing the linear stability results for various values of R, because the parameters G, α, β, and B are dependent upon $|T_0 - T_\infty|^q$.

The critical Grashof number G_{cr} steadily increases as R increases in the range $0.0 \leq R \leq 0.1333$, but, interestingly, further increase of R causes G_{cr} to decrease. However, at the same time the value of B* (i. e., B at G_{cr}) and B_{max} consistently decrease as R increases. The nose of a neutral stability curve shifts downward $B=0$ in the (G, B)-plane and its shape becomes sharper as R increases. As consequence of these observation, the upper limit of unstable frequencies with respect to R is predicted to be reduced and the flow is more unstable for lower frequencies, as R

Table 1 Values of η_{pI}, $-f_b''(\eta_{p.I})$, B^* and α^* for various values of R.

R	η_{pI}	$-f_b''(\eta_{p.I})$	G_{cr}	B^*	α^*
0.0	1.163	0.02847	41.89	0.19536	0.5928
0.05	1.086	0.02575	44.16	0.18027	0.5981
0.10	1.004	0.02574	46.55	0.16188	0.6034
0.11667	0.982	0.02693	47.22	0.15542	0.6081
0.1333	0.967	0.02925	47.69	0.14506	0.5969
0.15	0.971	0.03441	47.39	0.12955	0.5638
0.1515A	—	—	47.17	0.12646	0.5548
0.1515B	—	—	46.98	0.12449	0.5477
0.1515C	—	—	47.01	0.12451	0.5473

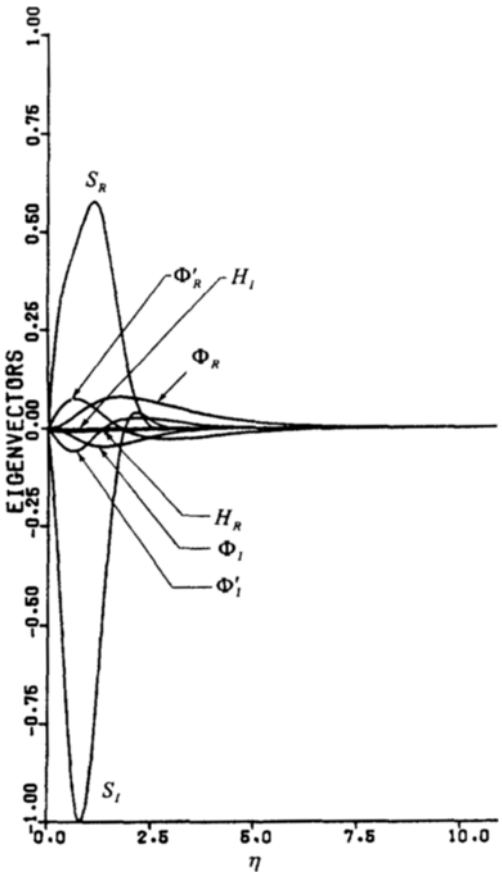

Fig. 11 Plots of eigenvector components vs η corresponding to the base flow at $R=0.05$ for $\alpha=0.6893$, $\beta=0.0570$, $G=44.60$ and $\eta_\infty=23.2$

increases from 0.0 to 0.1515.

It is also observed here that the location of a point of inflection in a base flow has a strong relationship to the critical Grashof number G_{cr}. As R increases from 0 to 0.1333 (and the heat transfer rate $-\theta_b'(0)$ decrease from 1.04697 to 0.8555), the location of the point of inflection $\eta_{p.I}$ in the profile of the velocity of the base flow f_b' shifts from $\eta_{p.I}=1.163$ at $R=0$ to $\eta_{p.I}=0.967$ at $R=0.1333$; at the same time the stress $-f_b''(\eta_{p.I})$ decreases (see Table 1). In addition, the present results show that the G_{cr} increases from 41.89 at $R=0$ to 47.69 at $R=0.1333$. But, as R increases from 0.1333 to 0.15, the $\eta_{p.I}$ increases from 0.967 to 0.971 and the corresponding $-f_b''(\eta_{p.I})$ increases from 0.02925 to 0.03441. Also, G_{cr} decreases from 47.69 at $R=0.1333$ to 47.39 at $R=0.15$. As the consequence of the above results, it is found that the shift of $\eta_{p.I}$ to $\eta=0$ with its weaker stress $-f_b''(\eta_{p.I})$ makes the velocity profile of the base flow more stable.

These phenomena are due to the effect of outside buoyancy force reversals. A slight increase of the downward buoyancy force in the outer region of the thermal boundary layer causes the base flow to be stable, but a further increase of this force causes the base flow to become unstable. Note, while buoyancy force reversals occur for $0<R\leq 0.15$, they are too weak to cause any reversals in the flow.

Figure 11 shows the typical shape of eigenvector components corresponding to near the nose of the neutral stability curves at $R=0.05$, which satisfy the accuracy criteria (10. a-b). In this figure, the real and imaginary parts of

eigenvector components (Φ, Φ', S, H) are normalized by their maximum values. In this figure, the maxima or minima of Φ, Φ', S, H occur very close to $\eta=0$. The locus of the peak positions associated with the large value of η_∞(up to 300 at $R=0.1515$) causes serious difficulties in solving the stability equations as R increases from $R=0$ toward $R=0.15$. (Note that the large value of η_∞ is inevitably required for accuracy in computation. This is due to the decrease in the value of f_b (∞) of the corresponding base flow (El-Henawy et al., 1982).)

In general, for $0\leq R\leq 0.1515$, the sensitivity of the eigenvalues α, β to the modified Grashof number G is so high near the nose of a neutral stability curve that the ranges between the upper and lower portions of a neutral stability curve in the (G, α) or (G, β)-plane are relatively much wider than the same ranges corresponding to a flow for $0.29181\leq R\leq 0.50$ (Hwang et al., 1993). Also, it is found that the critical Grashof number G_{cr} corresponding to the flow for $0\leq R\leq 0.1515$ is relatively higher (i. e., $G_{cr}\geq 41.89$) than the G_{cr} corresponding to the flow for $0.29181\leq R\leq 0.5$ (i. e., $G_{cr}\leq 22.81$). This significant difference is due to the characteristic features of the base flows associated with the outside buoyancy force reversals.

5. Discussion and Conclusion

The present numerical results indicate that when the parameter R is changed, the characteristic shape of the corresponding neutral stability curve is systematically changed : the critical Grashof number G_{cr} increases for $0\leq R\leq 0.1333$, but the upper limit of unstable frequency for flows B_{max} and the quantities β^* or B* (i. e., β or B at G_{cr}) decrease at the same time ; see Figs. 8 and 9. It is clear from our stability results that the unstable frequency range of disturbances becomes narrower as R increase. In other words, the band of corresponding favored frequency is reduced. Also, the neutral stability curves have blunter noses as R decreases. From the above tendencies, we conjecture that the corresponding spatial amplification contours would have more sharply pointed noses as R increases further toward 0.15. We also conjecture that the most favored frequency, which is the frequency that, according to theory, amplifies most quickly as the disturbance travels downstream, is decreased since both value of B^* and of B_{max} decrease as R increases. We believe these speculations are reasonable even though we have not performed computations to obtain the full details of the spatial amplification contours.

When we compared the stability results of the present work to the experimental data of Higgins and Gebhart (1982) at $R\simeq 0.0$ and $R\simeq 0.12$, the numerical results agree reasonably in a qualitative way with the experimental data. They observed that for $R\simeq 0$, the data lie at a frequency slightly higher than the theoretical frequency $B=0.36$. The range of frequencies which arose at each G location is broader than has been observed in warm water. Some intermittent bursts of turbulence were detected at $G=378$ for $R\simeq 0$. For $R\simeq 0.12$, the frequency bands lie closer to, and even below $B=0.36$. The band is narrower than that found at $R\simeq 0.0$. For $R\simeq 0.12$, Higgins and Gebhart (1982) observed a small amount of burst activity at $G=385$. From their observation, the point of transition to turbulence occurs some eight or nine times of G_{cr} downstream. Also, their observation implies that the neutral stability curve corresponding to $R=0.12$ lies left and shifts downward with respect to the neutral stability curve corresponding to $R=0$ (see also Table 1). Higgins and Gebhart also observed that at $G=417$, the disturbances corresponding to $R=0.12$ were more vigorous than those corresponding to $R\simeq 0$. They judged that disturbances corresponding to $R\simeq 0.12$ were amplified more quickly downstream than those corresponding to $R\simeq 0.0$.

From the results of our stabilizing calculation, it is found that there is a stabilizing or destabilizing effect due to the characteristics of the buoyancy force. In the range $0\leq R\leq 0.1333$, a small amount of the buoyancy force reversal causes the critical Grashof number to increase singnificantly. However, in the range $0.1333< R\leq 0.15$, a further increase of the outside buoyancy force reversal

causes the critical Grashof number to decrease. Namely, as R increases, the first instability of the flow occurs later for $0 \leq R \leq 0.1333$, then occurs sooner for $0.1333 < R \leq 0.15$.

At the same time the location of the single point of inflection $\eta_{p.i}$ (in the profile of the velocity of the base flow) and its stress-$f_b''(\eta_{p.i})$ strongly dependent upon the downward buoyancy force (in the outer portion of the thermal boundary layer) as mentioned in sec. 4. Further increase of this force causes an outside flow reversal which associated with two points of inflection to exist in the multiple-steady-state-solution region $0.15 < R \leq 0.1518$ found by El-Henawy et al. (1982), such as the two steady-states of the base flow at $R = 0.1515$ corresponding to the marks B and C in Figs. 3 and 6. From our results (as seen in Fig. 10 and Table 1), two points of inflection possess slightly lower values of the critical Grashof number than those with one. Thus, it is predicted that further increase of the downward buoyancy force cause the corresponding flow in the region $0.15 < R \leq 0.1518$ to become slightly unstable.

Acknowledgment

The author wishes to acknowledge support for this study by the Korea Science and Engineering Foundation under the grant 921-0900-035-2.

References

Ascher, U. Christiansen, J. and Russell, R. D., 1981, "Collocation Software for Boundary-Value Ordinary Differential Equations," *ACM Trans., Math software,* Vol. 7, pp. 209~222.

Bader, G. and Ascher, U., 1985, "A new Basis Implementation for a Mixed Order Boundary O. D. E. Solver," *Tech, Rep.* 85-11, Dept. of Computer Science, University of British Columbia, Vancouver, Canada.

Carey, V. P. and Gebhart, B., 1981, "Visualization of the Flow Adjacent to a Vertical Ice Surface Melting in Cold Pure Water," *J. Fluid Mech.,* Vol. 107, pp. 37~55.

Carey, V. P., Gebhart, B. and Mollendorf, J. C., 1980, "Buoyancy Force Reversals in vertical Natural Convection Flows in Water," *J. Fluid Mech.,* Vol. 97, pp. 279~297.

Deuflhard, P. and Bader, G., 1982, "Multiple Shooting Techniques Revisited," *Preprint No. 163,* Institute für Angewandte Math., University of Heidelberg.

El-Henawy, I., Gebhart, B., Hassard, B., Kasarinoff, N. and Mollendorf, J., 1982, "Numerically Computed Multiple Steady States of Vertical Buoyancy-Induced Flows in Cold Pure Water," *J. Fluid Mech.,* Vol. 122, pp. 235~250.

Gebhart, B., 1979, "Buoyancy Induced, Motions Characteristic of Applications in Technology," *Trans. ASME, J. Fluid Engng.,* Vol. 101, pp. 5~28.

Gebhart, B., Jaluria, Y., Mahajan, R. L. and Sammakiea, B., 1988, *Buoyancy-induced Flows and Transpot,* Heimisphere, N, Y.

Gebhart, B. and Mahajan, R. L., 1982, "Instability and Transition in Buoyancy Induced Flows," *Adv. Appl. Mech.,* Vol. 22, pp. 231~315.

Gebhart, B. and Mollendorf, J. C., 1977, "A New Density Relation for Pure and Saline Water," *Deep-Sea Res.,* Vol. 24, pp. 831~848.

Gabhart, B. and Mollendorf, J. C., 1978, "Buoyancy-Induced Flows in Water under Conditions in Which Density Extremes May Arise," *J. Fluid Mech.,* Vol. 89, pp. 673~707.

Higgins, J. M., 1981, "Stability of Buoyancy Induced Flow of Water Near the Density Extremum, Adjacent to a Vertical, Isothermal Surface," Doctoral dissertation, SUNYAB, Buffalo, N. Y.

Higgins, J. M. and Gebhart, B., 1982, "Measurements of Instability and Disturbance Growth in Vertical Buoyancy Induced Flows in Cold Water," *Int. J. Heat Mass Transfer,* Vol. 25, pp. 1397~1409.

Higgins, J. M. and Gebhart, B., 1983, "The Stability of Vertical Buoyancy Induced Flow in Cold Water," *Trans. ASME, J. Heat Transfer,* Vol. 105, pp. 767~773.

Hwang, Y., Kazarinoff, N. D. and Mollendorf, J. C., 1993, "Hydrodynamic Stability of Multiple Steady-States of Vertical Buoyancy-Induced Flows in Cold Pure Water," *Int. J. Heat Mass*

Transfer, Vol. 36, No. 2, pp. 423~435.

Qureshi, Z. H., 1980, "Stability and Measurements of Fluid and Thermal Transport in Vertical Buoyancy Induced Flows in cold water," Doctoral dissertation, SUNYAB, Buffalo, N.Y.

Qureshi, Z. H. and Gebhart, B., 1981, "Measurements of Fluid and Thermal Transport in Vertical Buoyancy Induced Flows in Cold Water," *Int. J. Heat Mass Transfer*, Vol. 24, pp. 1503~1511.

Qureshi, Z. H. and Gebhart, B., 1986, "The Stability of Vertical Thermal Buoyancy Induced Flow in Cold Pure and Saline Water," *Int. J. Heat Mass Transfer,* vol. 29, pp. 1383~1392.

Willson, N. W. and Vyas, B. D., 1979, "Velocity Profile Near a Vertical Ice Surface Melting into Fresh Water," *Trans. ASME J. Heat Transfer,* Vol. 10, pp. 313~317.